Magnetic neutron-scattering studies of $RbMnBr_3$

L. Heller, M. F. Collins, Y. S. Yang,* and B. Collier
Department of Physics and Institute for Materials Research, McMaster University, Hamilton, Ontario, Canada L8S 4M1
(Received 12 July 1993; revised manuscript received 17 September 1993)

$RbMnBr_3$ is an XY-like antiferromagnet on a distorted stacked triangular lattice. At low temperatures and fields we show by neutron scattering that there is an incommensurate ordered structure with magnetic Bragg peaks at $(h/8\pm\delta, h/8\pm\delta, l)$ where h and l are odd integers and $\delta=0.0183\pm0.0004$. At low temperatures, a field of 3 T applied along the a axis produces a first-order phase transition to a commensurate structure corresponding to $\delta=0$, so that the lattice parameter of the magnetic cell is eight times that of the nuclear cell. In addition to these two ordered structures, there is another incommensurate ordered phase found at high temperatures. The magnetic phase diagram shows a tetracritical point at zero field and $T=8.5\pm0.1$ K and a bicritical point at $H=2.55\pm0.05$ T and $T=7.8\pm0.1$ K. Inelastic neutron scattering was used to measure spin waves along the c axis and in the easy plane. The dispersion relations confirm that $RbMnBr_3$ is quasi-one-dimensional, with much stronger exchange along c than in the ab plane.

I. INTRODUCTION

Stacked hexagonal compounds of the form ABX_3, where B is a magnetic ion, have caused considerable interest because of the frustration found in the magnetic lattice.[1-3] These materials occur with one-dimensional magnetic chains along the c axis. The B ions interact through the bridging X ions with magnetic exchange constant J_1, which is much stronger than the interchain exchange J_2 so that at high temperatures the materials form quasi-one-dimensional magnets. Three-dimensional long-range magnetic order occurs at low temperatures resulting in diverse magnetic phases. When J_2 is antiferromagnetic and we have XY or Heisenberg spin interaction, neighboring moments tend to form equilateral triangles. This gives rise to a chiral degeneracy in the triangular sublattices. This additional degree of freedom may put the magnet into a new universality class.[3-5]

$RbMnBr_3$ crystallizes in a hexagonal lattice structure with $a=12.924$ Å and $c=6.547$ Å.[6] The Mn^{+2} ions are separated by a distance $c/2$ along the c axis. The structure of the manganese atoms within the basal plane is shown in Fig. 1. It is a distortion of the two-dimensional triangular lattice with one atom in three moved out of the plane by a distance $0.1088c$ along the c axis.[6] Each manganese atom with $z=0$ has six nearest-neighbor manganese atoms "in the plane" each with $z=0.1088c$, while each manganese atom at $z=0.1088c$ has as nearest "in-plane" neighbors three low ($z=0$) and three raised ($z=0.1088c$) manganese atoms. As we shall show from the inelastic-scattering measurements, the superexchange along c is two to three orders of magnitude stronger than in the ab plane. $RbMnBr_3$ has been observed to behave as a one-dimensional antiferromagnet at intermediate temperatures.[7] In zero applied field and below 8.6 K, $RbMnBr_3$ undergoes three-dimensional long-range antiferromagnetic ordering to an incommensurate structure with the spins in the ab plane.[7,8] The incommensurate structure seems to be based on the 120° commensurate triangular structure, since its magnetic Bragg scattering shows three peaks close to each commensurate peak. The three peaks are at 120° to each other in the ab plane around the commensurate $(1/3,1/3,l)$ position, preserving the threefold symmetry.

In this paper we investigate first the phase diagram of $RbMnBr_3$ in a field applied within the basal plane and show that there are three distinct ordered phases. The phase diagram includes both a tetracritical and a bicritical point. Then spin waves in $RbMnBr_3$ are studied and spin-wave dispersion curves are used in conjunction with spin-wave theory to produce values for the Heisenberg exchange constants along the c axis and in the ab plane.

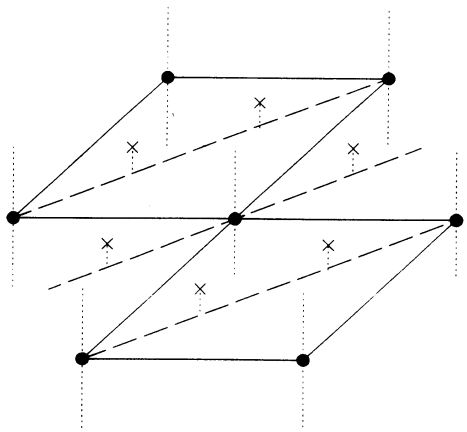

FIG. 1. The position of the magnetic manganese atoms in the basal plane of the hexagonal unit cell of $RbMnBr_3$. As well as the manganese atoms at the cell corners, there are also manganese atoms at $(1/3,2/3,z)$ and $(2/3,1/3,z)$ with $z=0.1088$, as marked by the crosses in the figure. This lattice is a distortion of the stacked triangular lattice where $z=0$.

II. EXPERIMENT

Two experiments were performed on a large cylindrical single crystal (1.5 cm diam by 3 cm long) of $RbMnBr_3$. The sample was grown by the Bridgeman technique in a vacuum ampoule using purified manganese bromide.

For the first experiment, the crystal was oriented with $(hh1)$ in the scattering plane and then placed in a helium cryostat. Measurements were taken between 4.2 and 12 K with the temperature stable to approximately ± 0.05 K. The crystal gave unstructured nuclear peaks with a mosaic spread of 0.4°. The measurements were carried out on the N5 triple-axis spectrometer of the NRU reactor at Chalk River Laboratories. An incident neutron energy of 3.497 THz was obtained from a silicon (111) monochromator and a pyrolytic graphite filter was added to further suppress second- and higher-order contamination. The horizontal collimation was 0.5° (monochromator to sample) and 0.25° (sample to analyzer). A silicon (111) reflection was used as the analyzer.

For the second experiment, the sample was placed in the same orientation into a vertical field magnetocryostat. The measurements were carried out on the C5 triple-axis spectrometer at the NRU reactor at Chalk River Laboratories. Data were again measured over the temperature range 4.2 to 12 K with applied magnetic fields varying from 0 to 5 T. A silicon (111) monochromator with a pyrolytic graphite filter was used to produce an incident neutron beam with energy 3.52 THz. For elastic-scattering experiments, the horizontal collimation was 0.20° (source to monochromator), 0.477° (monochromator to sample), and 0.273° (sample to analyzer). For the inelastic-scattering measurements no collimation was used both from source to monochromator and from monochromator to sample; from sample to analyzer the horizontal collimation was 0.477°. A silicon (111) reflection acted as the analyzer.

III. RESULTS

A. Elastic scattering

The elastic-scattering pattern develops new peaks below about 10 K, the exact temperature depending on the applied field as we will describe later. We have observed these peaks at (1/3,1/3,1), (2/3,2/3,1), (4/3,4/3,1), (1/3,1/3,3), and (2/3,2/3,3) and they correspond to a lattice of either $3a$ by $3a$ or $\sqrt{3}a$ by $\sqrt{3}a$ in the basal plane. We shall show later that we believe these peaks to be nonmagnetic in origin and to be due to a small nuclear distortion.

On cooling below 8.5 K in zero field an extra set of Bragg peaks appears in addition to the peaks of type (1/3,1/3,1). These are shown in Fig. 2 for scans $(\zeta\zeta 1)$ at 4.2 K. The upper panel shows a pair of peaks that can be indexed as $(1/8\pm\delta, 1/8\pm\delta, 1)$ with $\delta=0.0182\pm0.0003$. The lower panel shows the scattering pattern between $\zeta=0.28$ and $\zeta=0.42$. There are five Bragg peaks. One is at (1/3,1/3,1); the two peaks at higher values of ζ can be indexed as $(3/8\pm\delta, 3/8\pm\delta/1)$ with $\delta=0.0184\pm0.0003$, and the two peaks at lower values of ζ can be indexed as $(5/16\pm\delta/2, 5/16\pm\delta/2, 1)$ with $\delta=0.0184\pm0.0006$.

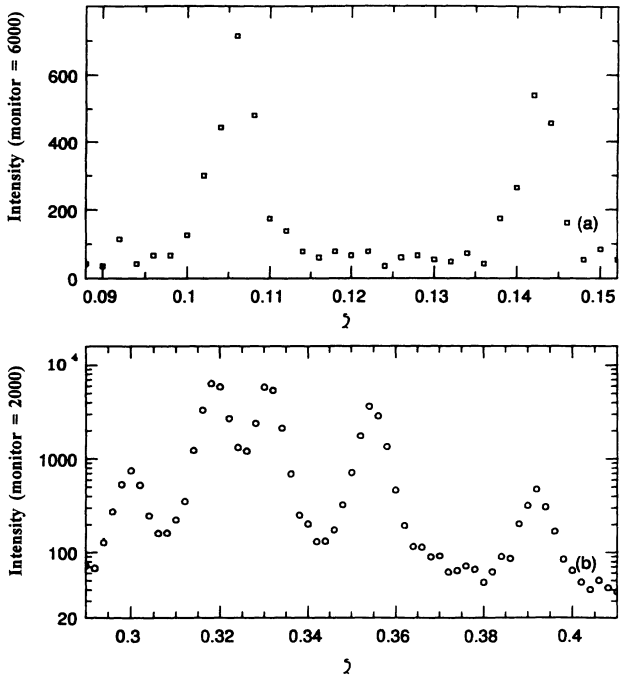

FIG. 2. Bragg-peak intensity along the $(\zeta\zeta 1)$ direction at $T=4.2$ K and $H=0$ T. In (a) incommensurate magnetic Bragg peaks of the form $(1/8\pm\delta, 1/8\pm\delta, 1)$ are seen. In (b) incommensurate magnetic Bragg peaks of the form $(3/8\pm\delta, 3/8\pm\delta, 1)$ and $(5/16\pm\delta/2, 5/16\pm\delta/2, 1)$ are seen along with the (1/3,1/3,1) Bragg peak. At this temperature and in this field the sample is in the low-temperature incommensurate phase with $\delta=0.0183\pm0.0004$.

Similar patterns are seen about the (1/3,1/3,3) and the (4/3,4/3,1) Bragg peaks and inverted patterns are seen about the (2/3,2/3,1) and the (2/3,2/3,3) Bragg peaks.

By rocking the crystal and cryostat out of the horizontal plane it was established that the incommensurate peaks are actually triplets of the form $(1/3+q, 1/3+q, 1)$, $(1/3+q, 1/3-2q, 1)$, and $(1/3-2q, 1/3+q, 1)$ where only the first of these peaks is in the $(\zeta\zeta 1)$ plane. The peaks seen at $(5/16\pm\delta/2, 5/16\pm\delta/2, 1)$ are the projection of the out of plane contributions of the peaks forming the triplet surrounding (1/3,1/3,1). The third member of the triplet is $(3/8\mp\delta, 3/8\mp\delta, 1)$.

The value of δ derived from the three pairs of peaks $[1/8\pm\delta, 5/16\pm\delta/2, 3/8\pm\delta]$ are the same within error, 0.0183 ± 0.0004, confirming our assignments of these magnetic peaks. Earlier work[7,8] on $RbMnBr_3$ has not identified this full set of magnetic Bragg peaks.

Data plots by Kawano, Ajiro, and Inami (Ref. 8) indicate that their experiment was performed with insufficient resolution to see all of the magnetic Bragg peaks. Data obtained by Kato *et al.* (Ref. 9) shows the existence of all of the incommensurate peaks between $\zeta=0.3$ and $\zeta=0.4$ along $(\zeta\zeta 1)$. If the peak at (1/3,1/3,1) is present in this data set, it is of weaker intensity than for our crystal and is not resolved.

Figure 3 shows scans taken in an applied magnetic field of $H=5$ T at $T=4.2$ K. The crystal has gone entirely

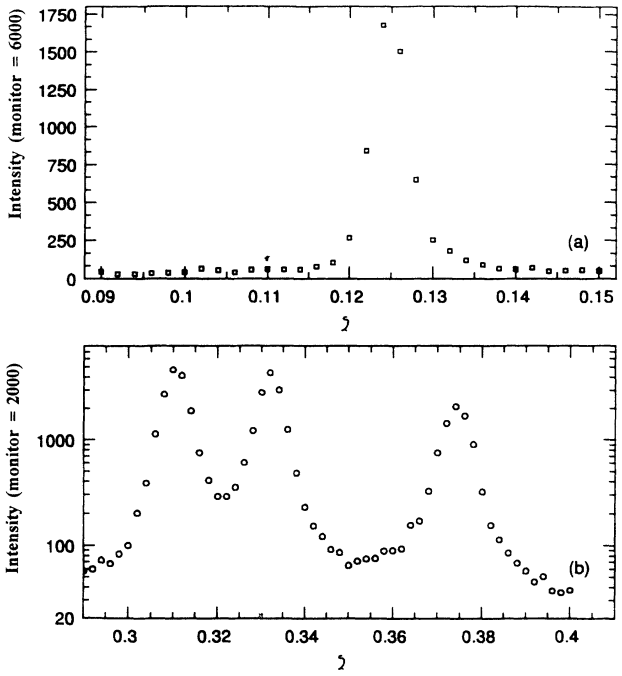

FIG. 3. Bragg-peak intensity along the $(\zeta\zeta 1)$ direction at $T=4.2$ K and $H=5$ T. In (a) a magnetic Bragg peak at $(1/8,1/8,1)$ is seen. In (b) magnetic Bragg peaks are seen at $(3/8,3/8,1)$ and $(5/16,5/16,1)$ together with the Bragg peak at $(1/3,1/3,1)$. The sample is now in the high-field phase.

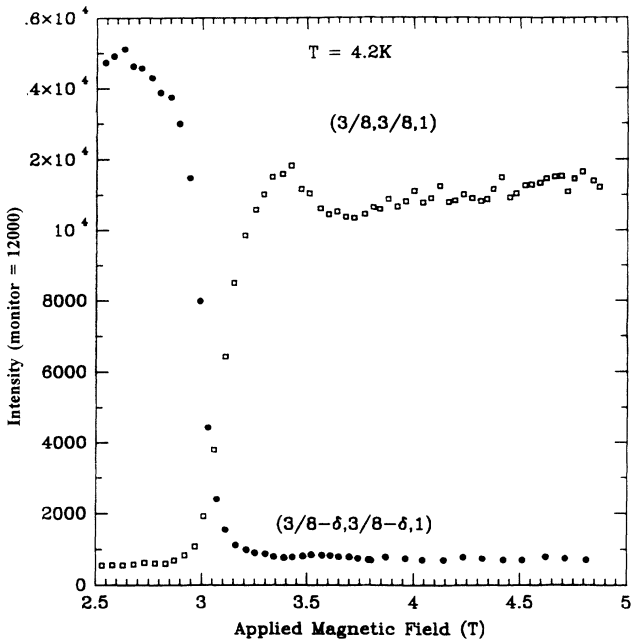

FIG. 4. Constant temperature scan of $(3/8-\delta,3/8-\delta,1)$ and $(3/8,3/8,1)$ at 4.2 K. The low-field and high-field phases cross over at about 3.05 T. Both scans were taken with field increasing.

into a new phase which we call the high-field phase. Figure 3(a) shows a peak at (1/8,1/8,1) and in Fig. 3(b) only the (1/3,1/3,1) peak together with peaks at (3/8,3/8,1) and (5/16,5,16,1) are seen. This pattern is the equivalent of that for the low-temperature phase with $\delta=0$.

Observations of the transition from the low-field state to the high-field state were made by varying the applied magnetic field at constant temperature. An example of the results of this type of scan is shown in Fig. 4 for $T=4.2$ K. There is a phase transition at $H=3.05$ T. The phase transition has an apparent width of about 0.2 T. The transition shows some hysteresis and the measurements shown correspond to increasing field. All fields for the phase transitions in this work are given for measurements taken with increasing field.

Figures 5–7 show how magnetic Bragg-peak intensities vary with respect to temperature at constant field. The plots in the three fields, 2.5, 2.75, and 3.25 T, are markedly different.

Figure 5 depicts the data at 2.5 T. There is evidence of two critical transitions for the peaks at $(3/8\pm\delta, 3/8\pm\delta,1)$ and at $(1/8\pm\delta,1/8\pm\delta,1)$: the first at 7.8 ± 0.1 K and the second at 8.8 ± 0.1 K. The first transition is from the low-temperature incommensurate phase to the high-temperature incommensurate phase. The second transition is from the high-temperature incommensurate phase to the paramagnetic phase.

The data at 2.75 T (Figure 6) very clearly shows transitions from the low-temperature phase to the high-field phase and from the high-field phase to the high-temperature phase. The peaks at $(3/8\pm\delta,3/8\pm\delta,1)$ and at $(1/8\pm\delta,1/8\pm\delta,1)$ disappear at 7.3 ± 0.1 K and reappear at 8.0 ± 0.1 K. These peaks are finally gone above 8.75 ± 0.1 K. Between 7.0 ± 0.1 K and 8.2 ± 0.1 K the (1/8,1/8,1) peak is seen, corresponding to the high-field phase.

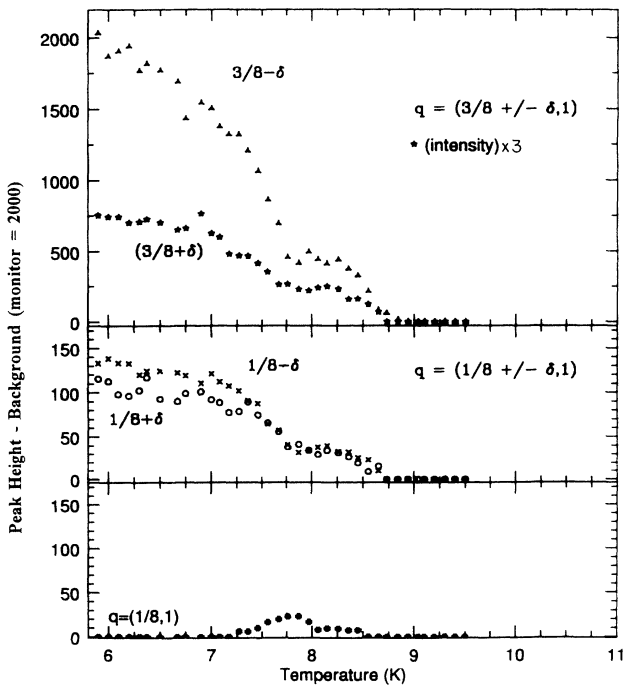

FIG. 5. Variation of magnetic Bragg-peak intensities with temperature in a magnetic field of 2.5 T. Two phase transitions are seen at 7.8 ± 0.1 K and at 8.8 ± 0.1 K.

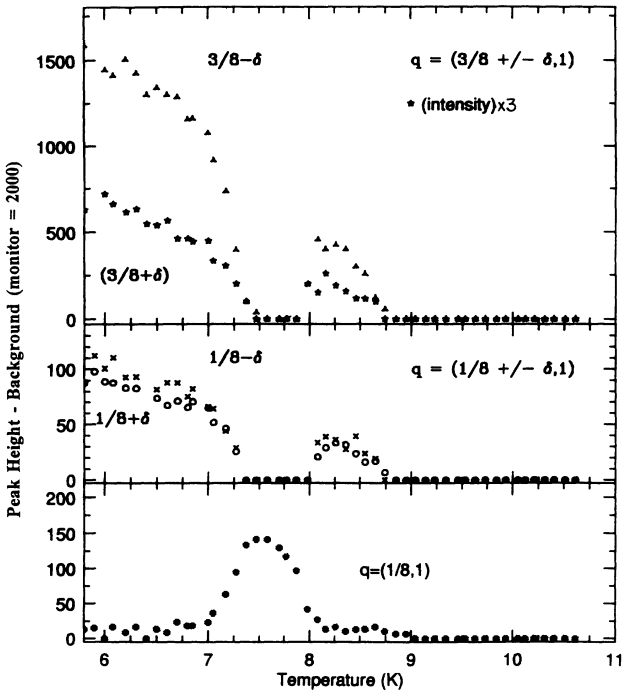

FIG. 6. Variation of magnetic Bragg-peak intensities with temperature in a magnetic field of 2.75 T. The incommensurate peaks undergo a first-order phase transition into the high-field phase around 7.3 K. Above 8 K the incommensurate peaks return.

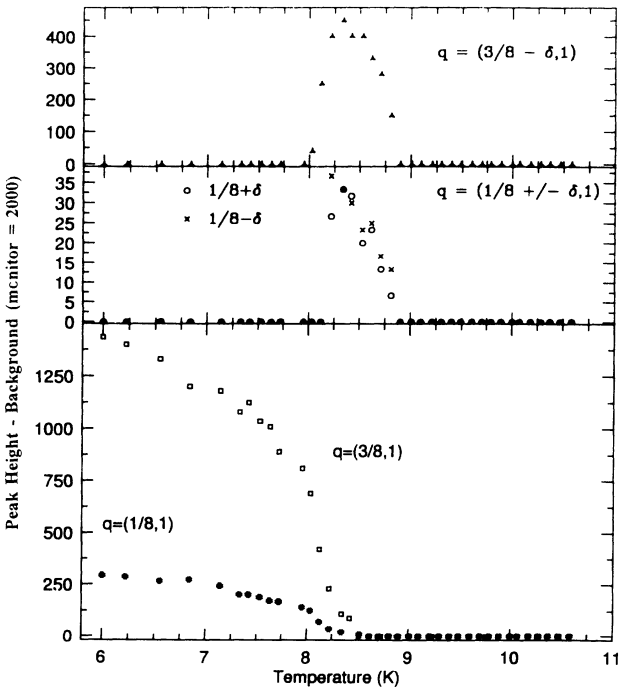

FIG. 7. Variation of magnetic Bragg-peak intensities with temperature in a magnetic field of 3.25 T. Peaks corresponding to the high-field phase are present below 8.25 K. Above this temperature there are incommensurate peaks present up to about 8.8 K.

Figure 7 shows data at 3.25 T where the low-temperature incommensurate phase is not seen. Below 8.2 ± 0.1 K the high-field phase is present as evidenced by the presence of peaks at (1/8,1/8,1) and (3/8,3/8,1). The phase transition at 8.2 K to the high-temperature phase is first order, though again somewhat broadened. From 8.2 ± 0.1 K to 8.9 ± 0.1 K the high-temperature incommensurate phase is seen, represented by peaks at $(1/8\pm\delta, 1/8\pm\delta, 1)$ and at $(3/8-\delta, 3/8-\delta, 1)$.

In Fig. 8 the intensity of the (1/3,1/3,1) peak is shown as a function of temperature in various applied fields. The behavior of this peak is very similar in each applied field which indicates that the commensurate peak is only weakly affected by the applied magnetic field. A comparison of Fig. 8 with Figs. 5–7 shows that there is no evidence that the magnetic phase transitions have any effect on the intensity of the commensurate peak. Figure 9 is a phase diagram for the phase in which Bragg peaks such as (1/3,1/3,1) are present. Its behavior is markedly different from that of similar peaks arising from a triangular magnetic ordering as is found in similar compound, $CsMnBr_3$.[3] We believe that it is unlikely that this peak is magnetic in origin, since if it were magnetic it would imply the simultaneous existence of two independent magnetic structures with large magnetic moments in the same crystal. The (1/3,1/3,1) Bragg peak does come from the whole crystal volume. We conclude that it is more likely that the peak arises from a nuclear distortion.

Using temperature scans of the incommensurate peaks at constant field and field scans at constant temperature we were able to map out the magnetic phase diagram for $RbMnBr_3$ (Fig. 10). In this figure the crosses (×)

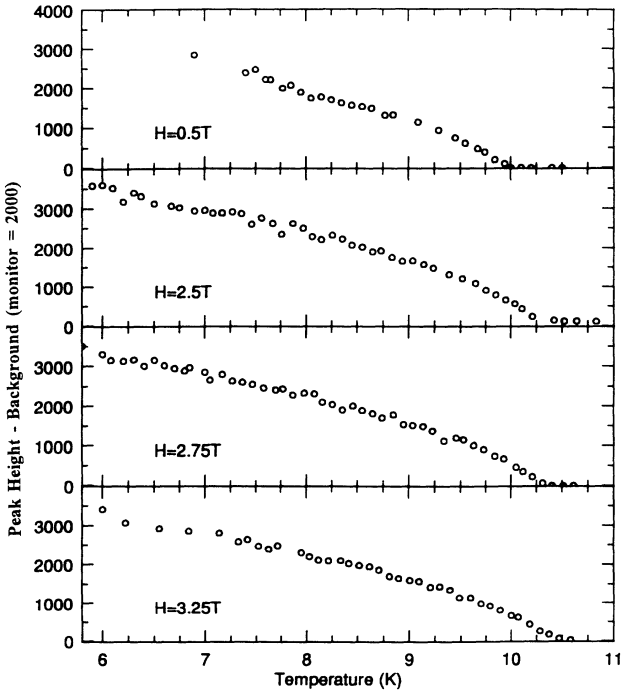

FIG. 8. Variation of the (1/3,1/3,1) peak in various applied fields. There is very little change in T_c as the field is increased and no perturbation in intensity at the various phase transitions shown in Figs. 8–11.

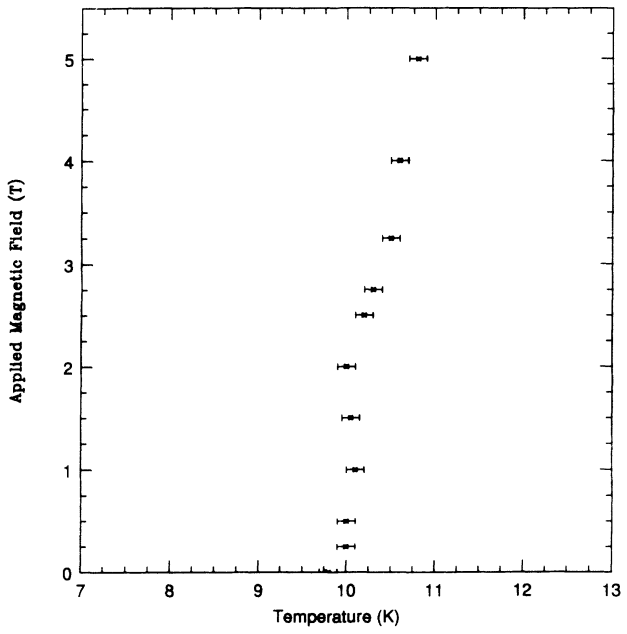

FIG. 9. Magnetic phase diagram for the (1/3,1/3,1) peak in $RbMnBr_3$. All points represent critical phase transitions.

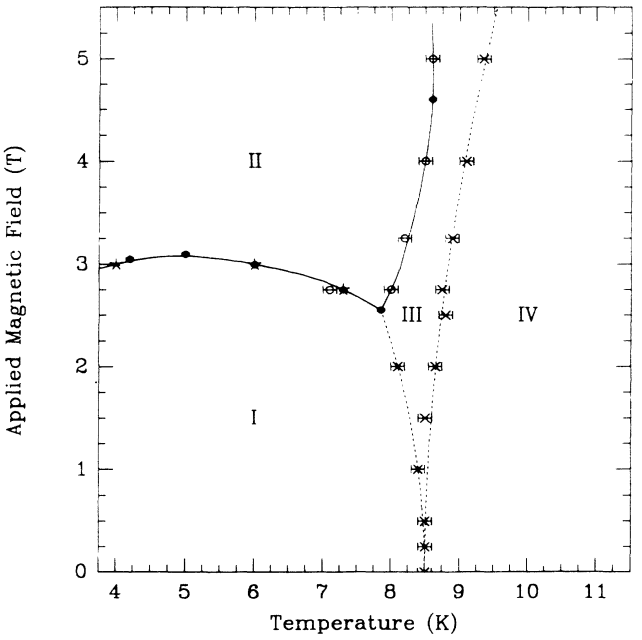

FIG. 10. Magnetic phase diagram for $RbMnBr_3$. Critical phase transitions are represented by crosses (x). All other transitions are first order either from constant temperature scans of (3/8,3/8,1) (closed circles) or $(3/8-\delta,3/8-\delta,1)$ (stars) or from constant field scans (open circles). Phase I is the low-temperature incommensurate phase, phase II is the high-field phase, phase III is the high-temperature incommensurate phase, and phase IV the paramagnetic phase. The broken lines are the results of least-squares fits of the critical temperatures at finite field according to Eq. (6). The continuous lines are guides to the eye that mark first-order phase transitions.

represent critical temperatures derived from constant field scans, hence we have lines of critical points from (7.8 K, 2.55 T) to (8.5 K, 0 T) and from (8.5 K, 0 T) to (9.3 K, 5 T). The other points on the diagram are all first-order points taken from constant temperature scans of either (3/8,3/8,1) or $(3/8-\delta,3/8-\delta,1)$ (closed circles, stars) or from constant field scans (open circles). Lines of first-order points extend from (3.8 K, 2.97 T) to (7.8 K, 2.55 T) and from (7.8 K, 2.55 T) to (8.8 K, 5 T). The point at $T=7.8\pm0.1$ K and $H=2.55\pm0.05$ T exists where a line of critical phase transitions meets two lines of first-order transitions, thus it is a bicritical point.[10] The point at $T=8.5\pm0.1$ K and $H=0$ T is a tetracritical point (i.e., the point at which four critical lines meet). A similar tetracritical point has been observed in $CsMnBr_3$.[3]

The phase diagram contains four distinct phases numbered I, II, III, and IV in Fig. 10. Phase I is the low-temperature incommensurate phase, phase II is the high-field phase, phase III is the high-temperature incommensurate phase, and phase IV is the paramagnetic phase. In all of phases I, II, and III the crystal has trigonal or hexagonal symmetry; the scattering pattern never corresponds to orthorhombic or lower symmetry.

Bhazan *et al.*[11] used measurements of magnetization to infer the phase diagram of $RbMnBr_3$. Their data indicates anomalies in the magnetization corresponding to the phase boundaries that we see with the exception that there is no anomaly at the boundary between phases II and III. Because of this they are unable to locate this boundary or the bicritical point. Except for this their general picture is in agreement with Fig. 9, though they locate the transition from phases I to II at a field of 3.75 T at 4.5 K, while we locate it at 3.05 ± 0.1 T. Kato *et al.*[9] used neutron-diffraction methods to locate this boundary and find a first-order phase transition at 2.9 T, which is close to the value that we find. Kato *et al.* also suggest that there is another phase transition at 4.0 T and 4.2 K corresponding to the weak minimum that we see in the intensity of (3/8,3/8,1) in Fig. 4 at 3.7 T. Although the two experiments both show ill-defined minimum in the intensity of the (3/8,3/8,1) magnetic peak, we have no reason to associate this with a phase transition. At all fields above 3.0 T our low-temperature Bragg profiles are centered at the commensurate positions $(n/8,n/8,l)$ with n and l odd. A scan along $(\xi\xi1)$ taken at 4.2 K in a field of 3.25 T showed a scattering pattern identical to Fig. 3, a scan of the sample in a field of 5 T. Figure 1 of Kato *et al.* seems to be in accord with out observations and we do not understand their assignment of an extra phase in the phase diagram.

The high-field phase shows some of the characteristics of a spin-flop phase but it is a surprise that it should be commensurate based on such a large cell ($8a$ by $8a$). The low-temperature and the high-temperature phases resemble each other in that both contain peaks at $(3/8\pm\delta,3/8\pm\delta,1)$ and $(1/8\pm\delta,1/8\pm\delta,1)$. Figure 11 shows how the value of 2δ changes with temperature in the various applied fields.

In the low-temperature phase at low fields (0, 2, and 2.5 T) the value of 2δ is constant until we near the phase boundary where 2δ begins to drop off. This dropoff is

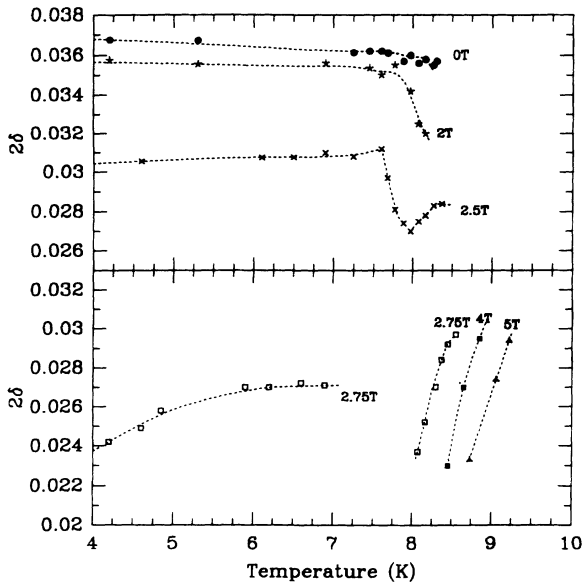

FIG. 11. Plot of 2δ versus temperature for various fields. 2δ is defined in Fig. 12. In phase III (high temperature) the value of 2δ increases rapidly with temperature, while in phase I (low temperature) the value of 2δ only varies weakly with temperature. The lines drawn are meant to serve as guides to the eye.

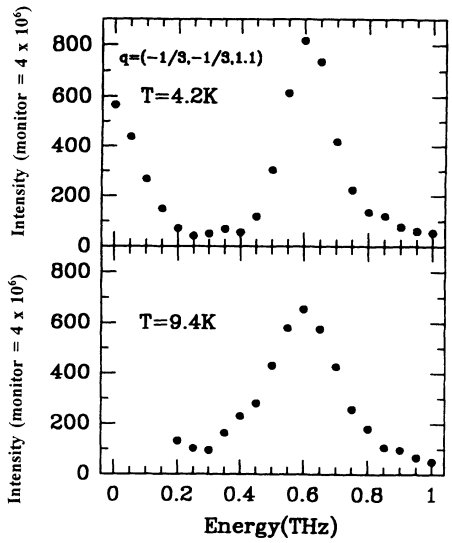

FIG. 12. Spin waves in $RbMnBr_3$ at 4.2 and 9.4 K with no magnetic field applied. Both spin waves were measured at $\mathbf{q}=(-1/3,-1/3,1.1)$.

small at low fields but becomes pronounced at higher fields. The data at 2.5 T shows a decrease in 2δ followed by an increase after the high-temperature phase is entered. At 2.75 T the value of 2δ is low at low temperatures and then plateaus before the crystal enters the high-field phase. Upon entering the high-temperature phase 2δ increases rapidly with increasing temperature. Similar behavior is observed in the high-temperature phase at 4 and 5 T. We conclude that in the low-temperature phase 2δ is only weakly dependent on temperature, while in the high-temperature phase the temperature dependence is more pronounced.

B. Inelastic scattering

Spin waves were measured both along the c axis and in the easy plane. All measurements taken along c were in zero field. Some spin waves along c are shown in Fig. 12 at 4.2 and 9.4 K for $\mathbf{q}=(-1/3,-1/3,1.1)$. At both temperatures the spin waves are well defined with frequency 0.61 ± 0.01 THz at 4.2 K and 0.60 ± 0.01 THz at 9.4 K. At 4.2 K the full width at half maximum is 0.18 THz and at 9.4 K this width has increased to 0.24 THz. The dispersion relation along the c direction at 4.2 K is given in Fig. 13. The line drawn in the figure is given by the following expression:

$$E=\{[1.99\sin(\pi q)+0.04\sin(2\pi q)]^2+0.22^2\}^{1/2}\ \text{THz}\ . \tag{1}$$

Hence we find that $J_1=-0.199\pm0.003$ THz, where J_1 is the Heisenberg exchange constant between neighboring manganese atoms along c and $J_3=0.004\pm0.003$ THz where J_3 is the Heisenberg exchange constant between second-nearest-neighbor manganese atoms along c. In $CsMnBr_3$, Collins and Gaulin have found $J_1=-0.213\pm0.003$ THz.[12] At $q_z=0$ we have a spin-wave energy of 0.22 ± 0.01 THz.

Figure 14 shows spin waves in the easy plane at 4.2 K and in zero field. The scans at $\mathbf{q}=(0.780,0.780,1)$ and at $\mathbf{q}=(0.820,0.820,1)$ show two spin waves superimposed on a large background. The spin-wave dispersion curve for the easy plane of $RbMnBr_3$ at 0 T and 4.2 K is shown in Fig. 15. The fits to the curves were drawn using the expressions for the spin-wave energies given by Kadowaki, Hirakawa, and Ubukoshi[13] for the stacked triangular lattice with a ground state that is a triangular arrangement of moments in the xy plane. The three branches are defined using the following equations:

$$h\omega_q=4S(|J_1|[|J_2|\{3+2f(h,k)\}+D])^{1/2}\ , \tag{2}$$

$$h\omega_q=4S[J_1J_2\{3-f(h+1/3,k+1/3)\}]^{1/2}\ , \tag{3}$$

$$h\omega_q=4S[J_1J_2\{3-f(h-1/3,k-1/3)\}]^{1/2}\ , \tag{4}$$

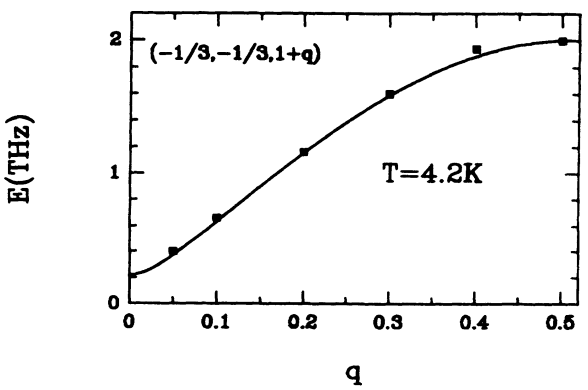

FIG. 13. Spin-wave dispersion relation along the c axis at 4.2 K. The line fitted to the curve is given in Eq. (1).

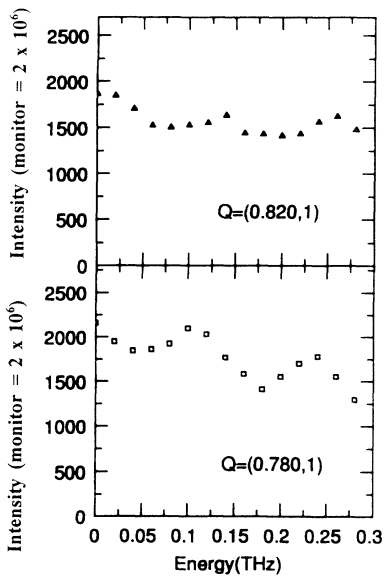

FIG. 14. Spin waves in the easy plane of $RbMnBr_3$ at 4.2 K with no magnetic field applied. Two spin waves are apparent at both $\mathbf{q}=(0.820,0.820,1)$ and at $\mathbf{q}=(0.780,0.780,1)$.

where

$$f(h,k)=\cos(2\pi h)+\cos(2\pi k)+\cos(2\pi)(h+k)) \quad (5)$$

for a spin wave vector $\mathbf{q}=(h,k,l)$. J_2 is the exchange constant between nearest-neighbor manganese atoms in the plane and D is the single-ion anisotropy parameter.

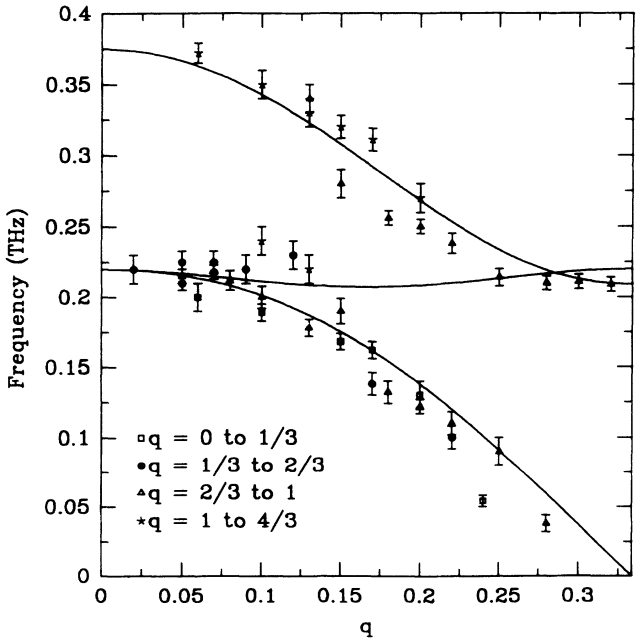

FIG. 15. Spin-wave dispersion relation in the easy plane at $T=4.2$ K with no applied magnetic field. The lines are the prediction of a model with nearest-neighbor exchange in the plane, $J_2=0.000\,54\pm0.000\,05$ THz and single-ion anisotropy parameter $D=0.0022\pm0.0001$ THz.

In this model, J_3 is assumed to be zero. J_2 is $-0.000\,54\pm0.000\,05$ THz and D is 0.0022 ± 0.0001 THz.

The Hamiltonian for the distorted triangular antiferromagnet $RbMnBr_3$ is unknown. The fit shown is a crude attempt to represent the spin-wave energy by energies developed from a Hamiltonian for an undistorted lattice with commensurate structure. The fit to the data is reasonably good, though there is evidence that the uppermost mode may actually be split into two branches.

In the undistorted commensurate triangular structure $CsMnBr_3$ a similar fit done by Gaulin, Collins, and Buyers[14] shows good agreement with theory. In that paper the uppermost mode is identified as the out-of-plane fluctuation (zz) and the two lower modes are identified as the in-plane and out-of-plane rotations within the easy plane [(xy) modes].

As predicted, the interactions along c are much stronger than those in the easy plane. $J_1/J_2\approx368$ as compared to $J_1/J_2\approx463$ for $CsMnBr_3$ (Ref. 13) and $J_1/J_2\approx200$ in $CsMnI_3$ (Ref. 2).

A comparison of the energies of the spin waves in the easy plane at the Néel temperature (T_N) with those at 4.2 K showed that the low-temperature spin waves occurred in all cases at a higher energy than those viewed at the same $\mathbf{q}$ at T_N. This is unlike what was seen in $CsMnBr_3$ in which the spin-wave energies at T_N were the same or slightly higher than those at low temperatures.[15]

Figure 16 shows the dispersion curve for the spin waves in the easy plane at 4 T. The lines drawn on the figure serve as guides to the eye. The plot is similar to the data in zero field (Fig. 15) with the upper branch reduced in frequency by about 20% and the lower branch by about 10%.

In Fig. 17 we see a spin wave present at 4.2 K in zero

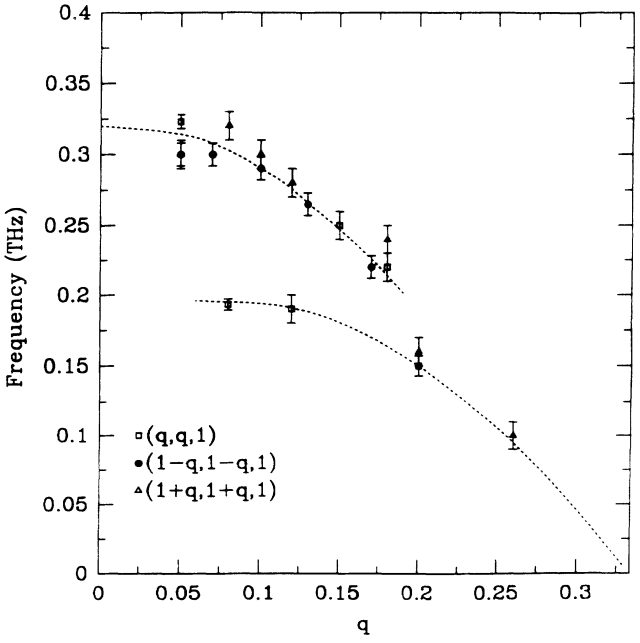

FIG. 16. Spin-wave dispersion relation in the easy plane at $T=4.2$ K and in a magnetic field of 4 T. Two branches are seen. The lines drawn are guides to the eye.

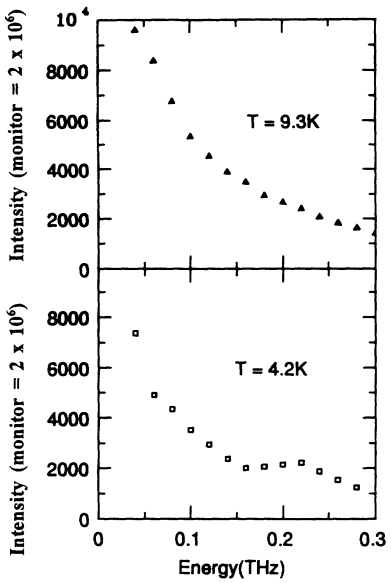

FIG. 17. Spin waves with $\mathbf{q}=(0.6,0.6,1)$ in $RbMnBr_3$. The spin wave at 4.2 K disappears at 9.3 K, a temperature at which the (1/3,1/3,1) peak is still present.

applied field for $\mathbf{q}=(0.6,0.6,1)$. At 9.3 K the spin wave has disappeared. The same result was found at a number of other wave vectors within the basal plane ($hh1$). Below 9.8 K in zero field the (1/3,1/3,1) peak is present but the excitations within the basal plane correspond to what is expected for a paramagnet. This supports our thesis that the (1/3,1/3,1) reflection is nonmagnetic.

IV. CONCLUSIONS

Elastic-scattering measurements in applied magnetic fields revealed that there are four magnetic phases of $RbMnBr_3$: a low-temperature incommensurate phase, a high-field commensurate phase, a high-temperature incommensurate phase, and a paramagnetic phase. The commensurate phase involves a lattice of size $8a$ by $8a$ in the ab plane. Both incommensurate phases show triplets of magnetic Bragg peaks centered on positions in the reciprocal lattice with $h=k=n/8$, where n is an odd integer. The high-field phase shows some characteristics of a spin-flop phase. There is a bicritical point in the phase diagram at $T=7.8$ K and $H=2.55$ T and a tetracritical point at $T=8.5$ K and $H=0$ T. Lines of both first order and critical points exist.

Plumer, Caillé, and Hood[16] have used Landau theory to investigate the phase diagram of antiferromagnets on a stacked triangular lattice. They show that a rich variety of phase diagrams may be possible, one of which is observed for $RbMnBr_3$ [Fig. 5(a) of Ref. 15]. The one difference is that the phase transition from the high-field to the high-temperature phase is predicted to be critical rather than first order. Loison and Diep[17] have predicted that phase transitions from a low-temperature phase to an intermediate phase are first order, though possibly only very weakly so. We have no evidence that the phase transition from the low-temperature incommensurate phase to the high-temperature incommensurate phase (phase I to III in Fig. 10) is anything but critical, however the high-field phase transition (phase II to III in Fig. 10) is first order as is that from phase I to III.

The broken lines drawn in the phase diagram (Fig. 10) are the results of least-squares fits of the critical temperatures at finite field according to the power-law behavior predicted[3] near the tetracritical point:

$$\frac{T_i(H^2)-T_N}{T_N}\alpha(H^2)^{1/\Psi_i}. \tag{6}$$

The Ψ_i's are the crossover exponents appropriate to the phase boundaries. The fit gives $\Psi_{\text{I-III}}=1.00\pm0.35$ and $\Psi_{\text{III-IV}}=1.07\pm0.25$, so that within experimental error $\Psi_{\text{I-III}}=\Psi_{\text{III-IV}}=\phi\approx1.0$. Kawamura, Caillé, and Plumer[18] predicted for the similar compounds $CsMnBr_3$ and $CsNiCl_3$ that $\phi=1.04$ and 1.06, respectively. $RbMnBr_3$ agrees with the hypothesis that both critical lines near the tetracritical point are scaled by a common exponent ϕ. This was not found to be the case experimentally for $CsMnBr_3$.[3] Zhang, Saslow, Gabay, and Benakli[19] and Kawamura[20] have looked at the effects of the lattice distortion, as shown in Fig. 1, on the magnetic structure. They show that for nearest-neighbor interactions the structure will correspond to a magnetic unit cell $\sqrt{3}a\times\sqrt{3}a$. Extra terms are needed in the Hamiltonian to give the observed incommensurate structures.

Spin waves were measured along c and in the easy plane. A fit to the dispersion relation along c gave $J_1=-0.199\pm0.003$ THz and $J_2=0.004\pm0.003$ THz. A fit to the data in the easy plane which collapses the incommensurate structure to a commensurate triangular structure gives $J_2=-0.000\,54\pm0.000\,05$ *THz and* $D=0.0022\pm0.0001$ *THz.*

ACKNOWLEDGMENTS

We would like to thank Chalk River Laboratories for the use of their facilities, especially Dr. Zin Tun and Mel Potter for technical assistance. We would also like to thank Dr. S. Kawano and Dr. O. Petrenko for useful discussions and for providing us with copies of their unpublished work. This work was supported by the Natural Sciences and Engineering Research Council of Canada.

*Also at AECL Research, Chalk River, Ontario, Canada K0J 1J0.

[1]M. Eibschutz, R. C. Sherwood, and F. S. L. Hsu, *Magnetism and Magnetic Materials, 1972 (Denver),* edited by C. D. Graham and J. J. Rhyne, AIP Conf. Proc. No. 10 (AIP, New York, 1973), p. 684.

[2]A. Harrison, M. F. Collins, J. Abu-Dayyeh, and C. V. Stager, Phys. Rev. B **43**, 679 (1991).

[3]B. D. Gaulin, T. E. Mason, M. F. Collins, and J. Z. Larese, Phys. Rev. Lett. **62**, 1380 (1989).

[4]H. Kawamura, J. Appl. Phys. **63**, 3086 (1988).

[5]T. E. Mason, B. D. Gaulin, and M. F. Collins, Phys. Rev. B **39**,

586 (1989).
[6]H. Fink and H.-J. Seifert, Acta Crystallogr. B **38**, 912 (1982).
[7]C. J. Glinka, V. J. Minkiewicz, D. E. Cox, and C. P. Khattak, *Magnetism and Magnetic Materials, 1972 (Denver)*, edited by C. D. Graham and J. J. Rhyne, AIP Conf. Proc. No. 10 (AIP, New York, 1973), p. 659.
[8]S. Kawano, Y. Ajiro, and T. Inami, J. Magn. Magn. Mater. **104-107**, 791 (1992).
[9]T. Kato, T. Ishii, Y. Ajiro, T. Asano, and S. Kawano (unpublished).
[10]M. F. Collins, *Magnetic Critical Scattering* (Oxford University Press, New York, 1989), p. 54.
[11]A. N. Bazhan, I. A. Zaliznyak, D. V. Nikiforov, O. A. Petrenko, S. V. Petrov, and P. A. Prozorova, Zh. Eksp. Teor. Fiz. **103**, 691 (1993) [Sov. Phys. JETP **76**, 342 (1993)].
[12]M. F. Collins and B. D. Gaulin, J. Appl. Phys. **55**, 1869 (1984).
[13]H. Kadowaki, K. Hirakawa, and K. Ubukoshi, J. Phys. Soc. Jpn. **52**, 1799 (1983).
[14]B. D. Gaulin, M. F. Collins, and W. J. L. Buyers, J. Appl. Phys. **61**, 3409 (1987).
[15]T. E. Mason, Y. S. Yang, M. F. Collins, B. D. Gaulin, K. N. Clausen, and A. Harrison, J. Magn. Magn. Mater. **104-107**, 197 (1992).
[16]M. L. Plumer, A. Caillé, and K. Hood, Phys. Rev. B **39**, 4489 (1989).
[17]D. Loison and H. T. Diep, J. Appl. Phys. **73**, 5642 (1993).
[18]H. Kawamura, A. Caillé, and M. L. Plumer, Phys. Rev. B **41**, 4416 (1990).
[19]W. M. Zhang, W. M. Saslow, M. Gabay, and M. Benakli, Phys. Rev. B **48**, 10 204 (1993).
[20]H. Kawamura, Prog. Theoret. Phys. Suppl. **101**, 545 (1990).